Distinct neural architectures underlie motor skill acquisition and transfer in human sensorimotor cortex

Theo Marins[1], Frederico Augusto Casarsa de Azevedo[2] and Guilherme Wood[1,3]

1. Institute of Psychology, University of Graz, Graz, Austria
2. McGovern Institute for Brain Research at MIT, Cambridge, United States
3. BioTechMed-Graz, Graz, Austria

Corresponding author: Guilherme Wood (guilherme.wood@uni-graz.at)
Author Contributions: TM designed the study; TM and FA analyzed data; GW administered and supervised the project; TM, FA, and GW wrote the paper.
Competing Interest Statement: The authors declare no competing interest.
Acknowledgements: This work was supported by the Austrian Science Fund FWF (ESP 397-BBL).

Abstract:

Motor learning typically emerges from repetitive practice but can also arise through transfer or generalization, where improvements extend to untrained actions. While training-based (training effect) and transfer/generalization-based (transfer effect) learning often result in comparable motor performance, little is known about the extent to which they share similar neural underpinnings or if they are two separate phenomena that rely on distinct cortical architecture. Here, we employed between-subject multivariate decoding of hyperaligned functional data obtained with high-field (7 Tesla) magnetic resonance imaging to characterize the universal neural codes underlying the training and transfer effects, and compared their resultant motor engrams in the sensorimotor cortex. We found that both learning mechanisms have reliable neural representations that are shared across individual brains, highlighting similar representational geometry despite idiosyncratic functional topographies. While their codes are embedded in overlapping cortical areas, the training effect has a more stable representation centered in the primary sensorimotor cortex, indicative of execution-level learning. In contrast, transfer effects elicited more abstract, variable codes in adjacent premotor and postcentral areas, suggesting flexible recombination of motor chunks. Moreover, the resultant cortical engrams shaped by them are particularly distinct in the left inferior part of the precentral sulcus, and in the right side of the superior part of the precentral sulcus, postcentral gyrus and postcentral sulcus. Our findings support the notion that motor skill learning is hierarchically organized in the sensorimotor cortex, and extend current models by revealing how training and transfer encode distinct, mechanism-dependent, and high-dimensional representations embedded in a neural code that is shared across brains.

Introduction

Motor learning often requires repetitive training, but it is also achieved through mechanisms of transfer of learning or generalization, in which improvements extend to untrained conditions (1). In motor training of finger-tapping sequences, this is detected as sequence-independent learning and suggests that both mechanisms of learning share similar neural resources (2, 3). In this way, neuroimaging studies have reported bilateral activation of M1/S1, cerebellum, and parietal regions during both training and transfer phases (2–4), but also have shown differential sensitivity to age (5) and task manipulations (6, 7), suggesting that the

two learning mechanisms are partially distinct at the neural level. This observation supports the hierarchical view of the sensorimotor system (8), which predicts that the repetitive selection of small movement elements leads to the formation of reusable representations of fragments of sequential movements, or chunks. In this way, evidence suggests that the low-level representation of sequential movements is stably encoded in the primary motor (M1) and somatosensory cortices (S1), while the intermediate-level representation of chunks relies on secondary sensorimotor areas (8–10).

In the present study, we investigated whether and to what extent the neural codes of training-based and transfer-based learning overlap, and described the motor engrams resulting from these processes. We used hyperalignment (11) to derive a common representational space that captures the basis functions that are shared among individuals. Hyperalignment leads to above-chance accuracy in decoding models applied to the visual system (12–16) by eliminating idiosyncratic, noisy, and task-unrelated neural patterns. We show that the neural representations of both mechanisms are shared across individual brains and are similarly distributed in the bilateral sensorimotor cortex. However, the training effect has a more robust and stable neural representation centered in the central sulcus, while the transfer effect shows weaker but reliable decoding accuracies in surrounding sensorimotor territories. Moreover, the motor engrams shaped by these different mechanisms of motor learning have distinct representations in the sensorimotor cortex, particularly in the left inferior part of the precentral sulcus, and in the right side of the superior part of the precentral sulcus, postcentral gyrus and postcentral sulcus. Altogether, our findings show that practice-based learning and transfer/generalization-based learning have distinct representations embedded in highly similar cortical architecture, which lead to diverging motor engrams that are shared among individual brains.

Results

We used 7-Tesla fMRI data to assess the multivariate patterns of brain responses to sequential finger-tapping movements of trained and untrained sequences. The participants (n=13, 9 females, mean age of 21.4 (std=2.36)) performed finger-tapping movements of 12 different sequences before and after five weeks of training, when six of them were practiced for around 4000 trials (Fig. 1A) (9). All sequences were matched by their difficulty level and consisted of nine digits long that were performed at the same pace with the five fingers of the right hand. Each sequence was executed twice in a row, three times within a run. Each session consisted of eight runs. A repeated-measures ANOVA revealed that the motor training protocol resulted in motor improvements in both trained and untrained sequences. The error probability of trained sequences decreased from 9.64% (mean, standard error = 0.48) to 5.42% (mean, standard error = 0.37) after the training protocol, whereas that of the untrained sequences went from 8.97% (mean, standard error = 0.47) to 6.81% (mean, standard error = 0.41).

We used hyperalignment to capture the response basis functions that are shared across individuals and project them into a common model, which has been shown to lead to above-chance level accuracy in between-subject classification tests (11). To avoid introducing noise to our analysis, we selected the first 12 pairs of trials (six of them of trained sequences, and six of untrained) executed without errors per run.

We built a common model of the sensorimotor cortex (17) using spherical searchlights by first setting aside the data from the test subject (Fig. 1B). The training data consisted of all runs but one of the remaining subjects, which was used to create the common space and train the decoder. Then, the left-out run of the test subject was aligned to the common space and used to test the decoder's accuracy. We repeated this procedure so that each run from each subject was used as test data (13 subjects x 8 runs = 104 folds). Importantly, we avoided overfitting by keeping apart the training and test data to build the common space and train the decoder (Fig. 1B). This procedure was conducted independently three times, modelling different aspects of motor behaviour. In two of them, we investigated the effect of time (before and after motor training) on the neural signatures of the execution of trained and untrained sequences, henceforth called 'training effect' and 'transfer effect', respectively. In addition, we explored the mechanism-specificity of the neural signatures after the motor training on both trained and untrained sequences (henceforth called 'resultant motor engrams').

The universal neural representations of training and transfer effects are distinct but similarly embedded in the sensorimotor cortex. The investigation of how the training and transfer effects are encoded in the sensorimotor cortex revealed a bilateral engagement of multiple areas (Figure 2A). The central sulcus showed divergent involvement in both mechanisms: while in the training effect it showed markedly high accuracy, learning encoded by the transfer effect is distributed outside the central sulcus, as revealed by the 95% confidence interval (Figure S1). We calculated the average decoding accuracy of suprathreshold vertices in each of the six cortical regions in each hemisphere and computed the main effects of condition (trained, untrained), cortical label (anterior and superior parts of the precentral sulcus, precentral gyrus, central sulcus, postcentral sulcus, and postcentral gyrus), and their interaction using a repeated-measures ANOVA. The effect of condition ($F(1, 12) = 36.12$, $p = 0.0001$) revealed that the training effect has higher decoding accuracy than the transfer effect ($t = 6.01$, $p < 0.001$; Cohen's $d = 1.18$). A significant main effect of cortical label was also found ($F(5, 60) = 2.62$, $p = 0.03$), suggesting that accuracy varied across different brain regions. Importantly, there was a significant interaction between condition and cortical label ($F(5, 60) = 15.08$, $p = 0.0000$). Pairwise t-test with false discovery rate (FDR) correction for multiple comparisons indicated that the central sulcus ($t=8.03$, $p=0.00002$), the precentral gyrus ($t=4.13$, $p = 0.002$), the superior ($t=4.61$, corrected $p=0.001$) and inferior ($t=4.84$, corrected $p=0.001$) parts of the precentral sulcus have higher decoding accuracy for the training effect, compared to the transfer effect. Given the distinct nature of each hemisphere on motor learning, we further explored how these codes are balanced between hemispheres using the laterality index (LI). For each sensorimotor cortical region, LI was obtained using the formula $LI = (R - L) / (R + L)$, where R and L are the average accuracy of the suprathreshold vertices in the right and left hemispheres, respectively (Figure 2B). Extreme (1 or -1) LI values indicate strong lateralized representations, while indices closer to zero point to a more balanced representation across hemispheres.

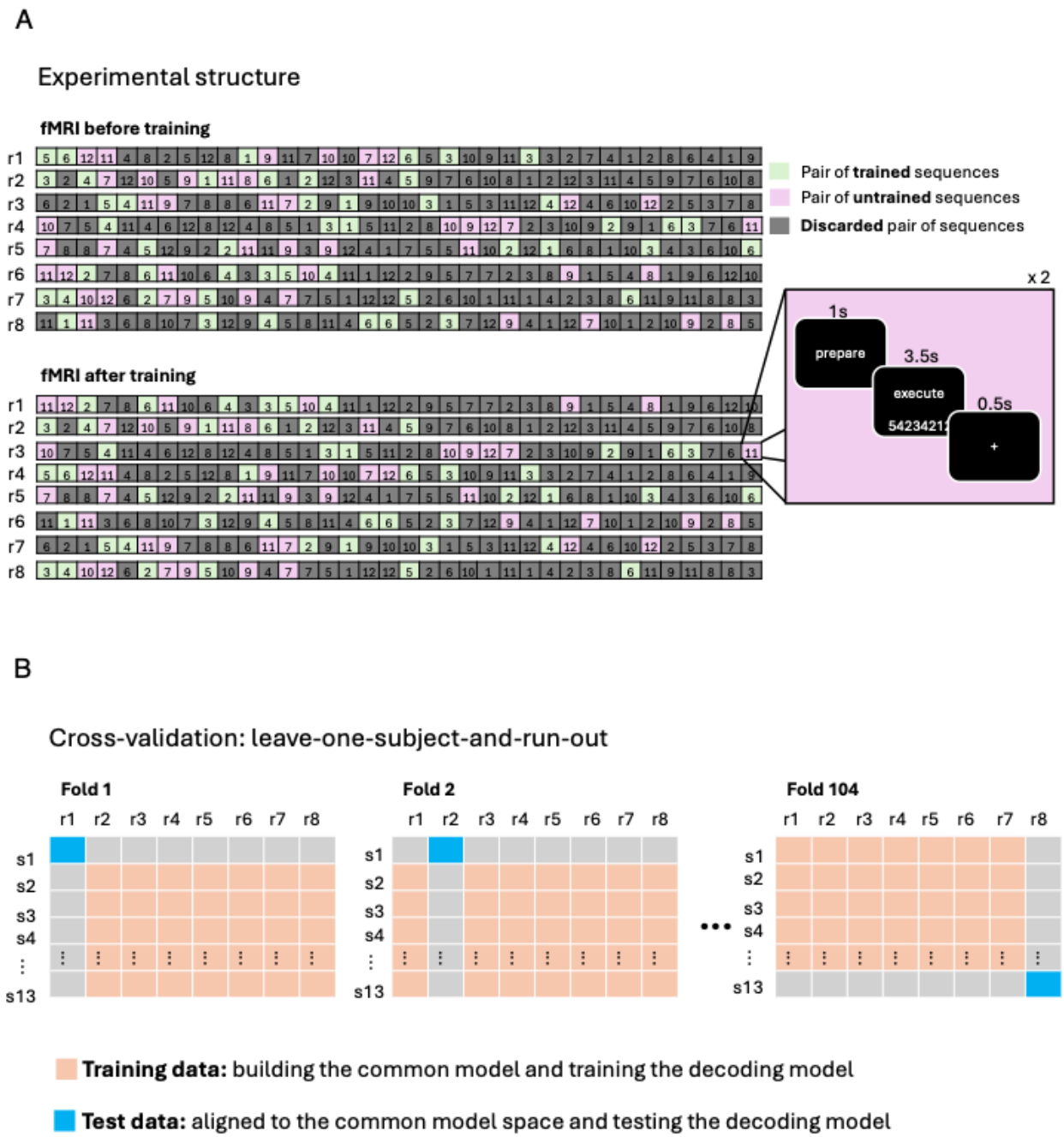

Figure 1. Experimental structure and cross-validation scheme. (A) Before and after the five-week training, participants (s1–s13) were scanned during the execution of 12 different sequences of finger-tapping movements. Each sequence was performed twice in a row (represented by a single square), three times per run, for eight runs (r1–r8). To reduce noise and task-unrelated signal, the first 12 pairs of sequences (six trained, green; six untrained, purple) were modeled using a surface-based first-level general linear model (GLM), and each square represents the resultant z-map of a pair of trials. Each trial consisted of 1s of preparation, followed by 3.5 s of execution (with visual aid) and 0.5s of inter-trial interval. Periods of rest (not shown) were added in-between trials. (B) The between-subject classification was performed by first setting aside the test subject. The train data consisted of all runs but one of the remaining subjects, which was used to create the common space and to train the decoder. Then, the left-out run of the test

subject was aligned to the common space and used to test the decoder's accuracy. We repeated this procedure so that each run from each subject was used as test data.

The training effect relied more on the right side (ipsilateral) of the postcentral sulcus and the superior part of the precentral sulcus, while it was preferentially left-lateralized in the inferior part of the precentral sulcus and the precentral gyrus. The transfer effect showed the same laterality pattern, in addition to a stronger encoding in the right postcentral gyrus. LI comparison showed no main effect of condition ($F(1, 12) = 0.17$, $p = 0.68$), but a significant effect of cortical label ($F(5, 60) = 34.26$, $p = 0.0000$). Even though there was an interaction between condition and cortical label ($F(5, 60) = 3.53$, $p = 0.007$), pairwise t-test with FDR correction did not reveal statistically significant differences between conditions within individual cortical labels. This suggests that the neural codes of both training and transfer effects have similar distributions over the bilateral sensorimotor cortex, despite different magnitudes.

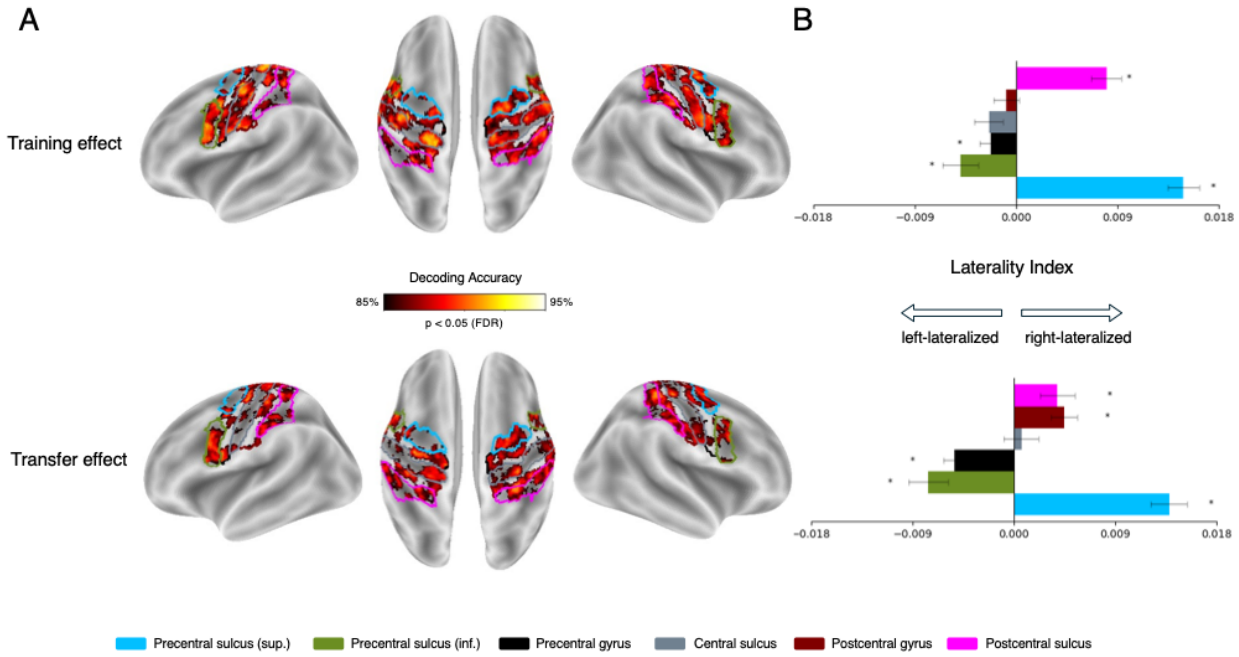

Figure 2. Decoding models for the training and transfer effects after hyperalignment. A) Brain maps showing decoding accuracy of the training (top) and transfer (bottom) effects. The brain maps show vertices that survived the permutation test ($p < 0.05$) and FDR correction (Benjamini-Hochberg). B) Laterality index of the neural codes of training (top and transfer (bottom) effects. Training and transfer effects were bilaterally encoded in the sensorimotor cortex, with significantly higher decoding accuracy for training in the central sulcus ($t=8.03$, $p=0.00002$), precentral gyrus ($t=4.13$, $p = 0.002$), and both parts of the precentral sulcus (superior: $t=4.61$, corrected $p=0.001$; inferior: $t=4.84$, corrected $p=0.001$.) Lateralization patterns differed across regions, but no overall laterality difference between conditions was found.

In addition to comparing the average accuracy between groups, we also directly contrasted both accuracy maps (Training vs. Transfer), vertex-wise. It revealed that most of the sensorimotor cortical regions showed stronger accuracy for the training effect (Figure 3). In the right hemisphere, all cortical labels except the postcentral gyrus showed higher decoding

accuracy for the training effect. In the left hemisphere, the superior part of the precentral sulcus and the central sulcus showed preferential encoding for the training effect, while the postcentral sulcus showed greater accuracy for the transfer effect.

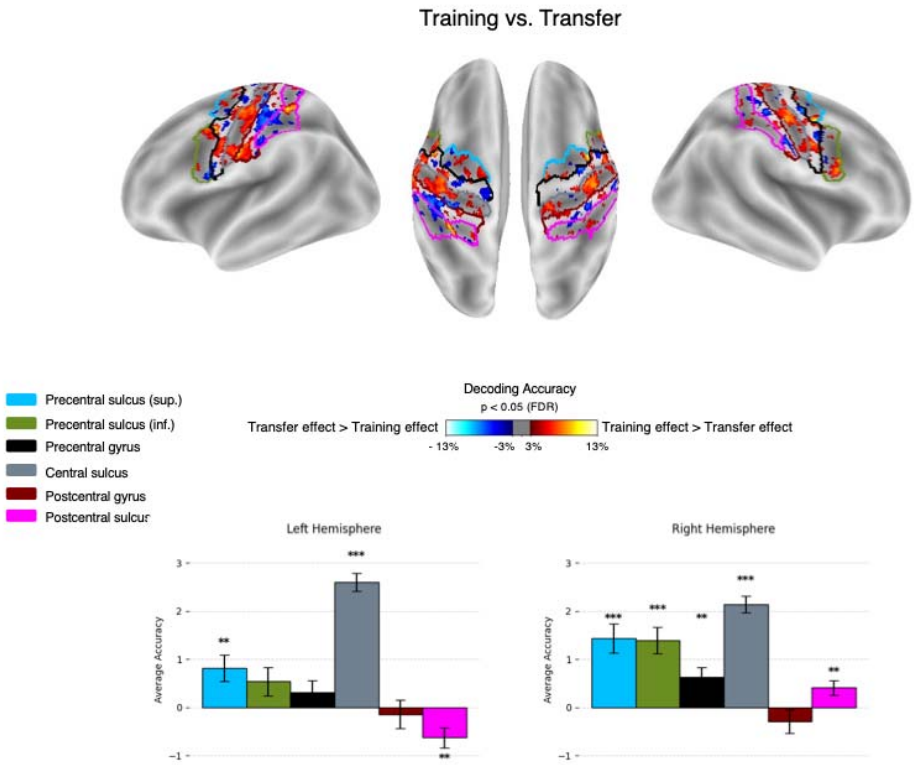

Figure 3. Direct comparison of the neural codes of training and transfer effects with hyperalignment. Red to yellow vertices indicate higher decoding accuracy for the training effect (Training > Transfer), while blue to cyan vertices indicate higher decoding accuracy for the transfer effect (Transfer > Training). The map shows vertices that survived a two-sided test, permutation testing, and FDR correction (Benjamini-Hochberg).

The resultant motor engrams are mechanism-dependent. After the motor training protocol, the mechanism by which motor learning occurred was decoded above chance in all cortical regions (Figure S1), with a clear shift towards the right hemisphere (Figure 4A). Specifically, the neural codes that resulted from the training and transfer effects were particularly distinct in the left inferior part of the precentral sulcus, and in the right side of the superior part of the precentral sulcus, postcentral gyrus, and postcentral sulcus. The multidimensional scaling plot (Figure 4B) displays the cosine dissimilarity in all sensorimotor cortical labels, showing that after motor training (blue and red squares), the representational patterns of both trained (red) and untrained sequences (blue) diverge from their pre-training configuration (blue and red circles), with trained sequences exhibiting a more pronounced shift.

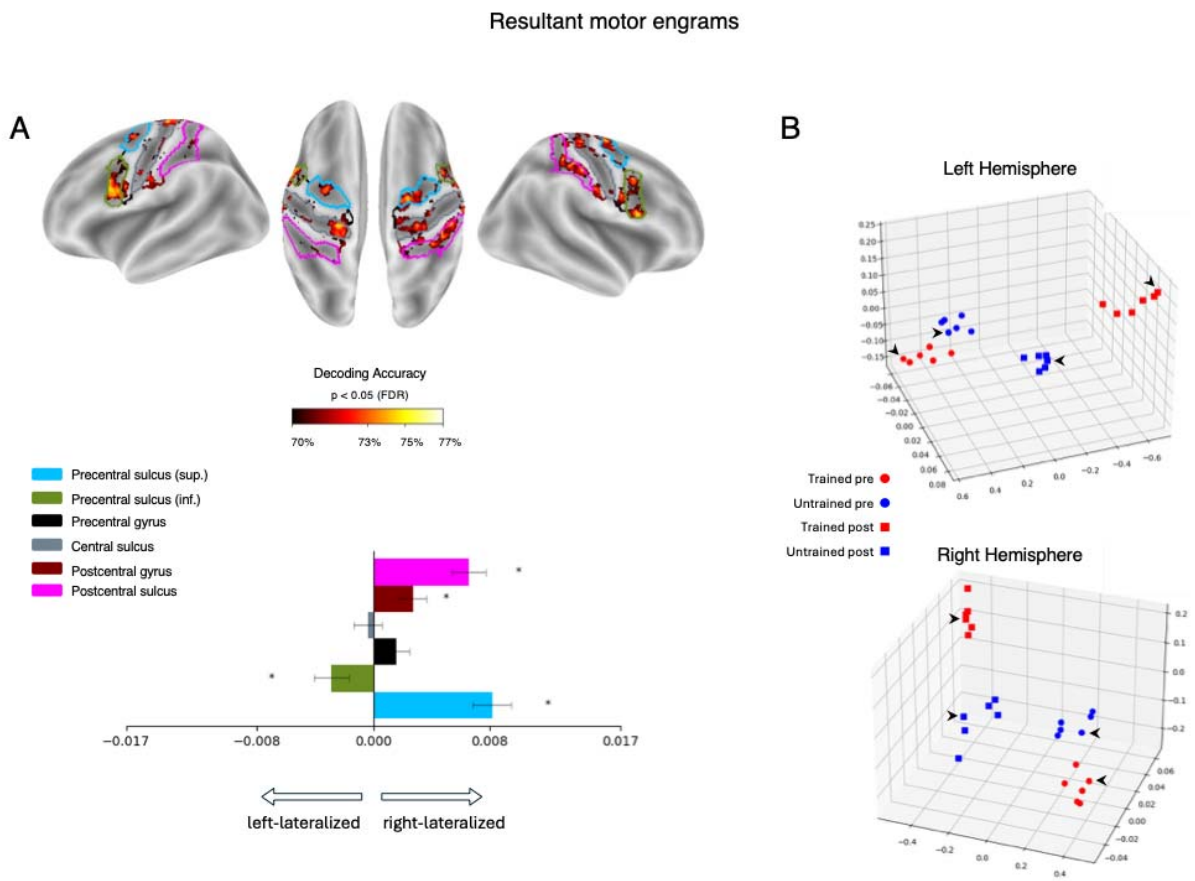

Figure 4. Decoding model for the resultant motor engrams. A) Brain maps showing decoding accuracy of the decoding model that compared the resultant motor engrams (top), revealing that the resultant motor engrams were decoded above chance across all regions, with stronger right-hemisphere involvement. The brain map shows vertices that survived the permutation test ($p < 0.05$) and FDR correction (Benjamini-Hochberg). The laterality index of the mechanism-specific neural codes (bottom). B) Multidimensional scaling plot of the cosine dissimilarity of trained (red) and untrained (blue) sequences performed before ("pre", circles) and after ("post", squares) motor training in the left (top) and right (bottom) hemispheres. Each data point in the plot represents the average cosine dissimilarity in one cortical region (a total of six cortical regions). Arrowheads highlight the data from the central sulcus. Notable pattern shifts emerged in the left inferior precentral sulcus and right superior precentral sulcus, postcentral gyrus, and sulcus.

Discussion

In the present study, we investigated the high-dimensional representation of the training-based and transfer/generalization-based learning of sequential finger-tapping movements. We found that (i) both mechanisms have distinct neural representations, embedded in an overlapping cortical landscape, that (ii) lead to two distinct motor engrams, (iii) which are shared across individual brains. Specifically, while the neural representations of both learning mechanisms are similarly distributed across hemispheres – right-lateralized in the superior part of the precentral sulcus and postcentral gyrus, and more pronounced in the left inferior part of the precentral sulcus and precentral gyrus –, the training effect showed stronger decoding

accuracy than the transfer effect all over the sensorimotor cortex, especially in the central sulcus, precentral gyrus and the superior and inferior parts of the precentral sulcus. A direct and vertex-wise comparison between the training and transfer effects reinforced these findings and highlighted the differential involvement of the central sulcus. Importantly, the motor engrams shaped by these mechanisms of motor learning are distinct, particularly in the right superior part of the precentral sulcus, postcentral sulcus and gyrus, and in the left inferior part of the precentral sulcus. Altogether, our findings support previous studies showing that both practice-based and transfer/generalization-based motor learning recruit similar cortical regions (2–5, 18). Importantly, we extend previous findings by demonstrating that these two learning mechanisms encode different neural content, resulting in distinct motor engrams, which reinforces the idea that training and transfer involve separate, though overlapping, processes. Reinforcing the model of hierarchical organization of motor skill learning, these findings suggest that repetitive training consolidates rigid, execution-focused representations in primary sensorimotor circuits, whereas transfer or generalization relies on dynamic, chunk-based coding in secondary areas.

Studies have shown that the sensorimotor cortex is differentially engaged over the course of a motor training protocol and in response to the transfer of learning, showing either activation increases and decreases, depending on the stage of the learning process (1, 9, 18–20). In motor learning, increased brain activity is commonly interpreted as the strengthening of neural circuits involved, whereas decreased activity is often interpreted as neural optimization or better processing efficiency (20–22). However, these fluctuations are difficult to interpret, as they likely reflect the summation of multiple complex neural processes occurring during motor learning (23). Moreover, simply reporting that certain brain regions display higher or lower activation after training does not provide meaningful information about the specific nature of their contributions to the task—it merely describes the extent of involvement, not its content. Therefore, investigating the content of cortical engagement during practice-based learning and transfer/generalization-based learning requires multivariate methods capable of decoding '*what'* is encoded, rather than merely quantifying the average level of activity (24). In this way, if the neural circuitry of the training and transfer effects were identical (if both learning mechanisms were, in fact, a single phenomenon), it would not be possible to decode them with multivariate and decoding analysis. Instead, we deepen the comprehension of the neural basis of motor learning by describing that the sensorimotor cortex is differentially involved in those processes. Illustrating this divergent neural representation throughout the motor training protocol, the multidimensional scaling plot highlights clear distinctions between activation patterns associated with training and those related to transfer.

The anatomical variability and idiosyncratic functional response of cortical structures are the main challenges that hamper between-subject classification (25) of neurophysiological data. Functional alignment using hyperalignment overcomes this by creating a high-dimensional model that represents the response-tuning functions that are common across individual brains (11, 24). In this type of approach, the cross-validation scheme is of extreme importance. Here, we avoided data leakage by keeping the train and test data apart for the common model estimation and decoder training. Thus, we can conclude that the only possible way to get above-chance decoder accuracy in our between-subject classification model is if both training and test data contain similar representation structures. Hence, our findings revealed the

existence of a shared, high-dimensional information space that represents motor learning achieved by two distinct mechanisms.

We showed that learning encoding via training effect relies robustly in the central sulcus, diverging from what happens in the transfer effect. This is consistent with the view that motor skill learning is structured in layers, from high-level action plans, through mid-level “chunks”, down to low-level muscle commands (8). Here, repetitive practice likely sculpted execution-level primitives in the primary sensorimotor cortex, reflecting the formation of stable, invariant neural codes that automate execution, which led to higher decoding accuracy across M1/S1. In contrast, transfer/generalization recruited more abstract, chunk-like representations in adjacent premotor/postcentral regions, which support flexible recombination. This interpretation is supported by our direct comparison between both learning mechanisms, which might indicate the formation of specialized and more stable neural circuits through repetitive training in the sensorimotor cortex, especially in M1/S1 (8, 9, 26, 27), whereas the transfer effect showed weaker but still reliable decoding accuracy in premotor/postcentral areas, representing the variability and less informative characteristics of the chunk-related neural codes (9, 26–28).

Motor engrams are known to support the execution and acquisition of skilled movements (29). Here, training and transfer effects led to two robust and different motor engrams, reinforcing that despite engaging similar cortical structures, their roles are different, thus representing distinct phenomena. These engrams were sufficiently distinct to be decoded with above-chance accuracy in all the sensorimotor cortical regions. Interestingly, the right (ipsilateral) hemisphere played a key role in decoding the learning mechanism, as the superior part of the precentral sulcus, and the postcentral gyrus and sulcus on the right side showed stronger accuracy than their contralateral counterparts. While ipsilateral activity of the sensorimotor cortex has been described in multiple studies (2, 3, 10, 26, 30–34), evidence of its contribution to motor learning is still under debate. According to the “interhemispheric competition” model, in which the ipsilateral sensorimotor cortex receives inhibitory inputs from the contralateral hemisphere (35), the ipsilateral brain activity during unimanual motor tasks is associated with impaired motor behavior, and suppressing it is beneficial for motor learning in healthy individuals (36, 37) and motor recovery after stroke (38–40). Likewise, stimulating ipsilateral M1 impairs motor learning (41). In contrast with this view, other studies point to a collaborative nature of ipsilateral activity that may occur through changes in the interhemispheric communication (42). Even though weaker, the ipsilateral sensorimotor cortex encodes finger movements (43, 44) and finger-tapping sequences (45), and stimulating these areas has been linked to a positive impact on motor learning (46).

While previous studies report stable sequence representations in contralateral M1 during motor learning (9, 26, 47), we observed strong bilateral M1/S1 encoding of the training effect. This apparent contradiction resolves when considering that our decoding approach was built to classify the neural states of finger-tapping movements before and after motor training in a sequence-independent manner, rather than describing sequence-specific features of skill encoding. Thus, we sought to characterize the temporal dynamics of the high-dimensional representations of motor sequence learning. In this way, our findings showed that the neural codes of the training effect rely on different parts of the sensorimotor cortex, but are centered in the central sulcus. In the same way, several plasticity mechanisms in M1 have been described

in response to motor sequence learning (48–52), although imaging studies revealed heterogeneous findings about the engagement of the contralateral M1 in motor sequence learning (3, 9, 23, 26, 27, 45, 53).

In conclusion, our study shows that the training and transfer effects have different neural codes embedded in a similar cortical topography, which are shared across individual brains. The training and transfer effects shape distinct motor engrams, reinforcing the idea of different mechanisms by which motor learning occurs. Importantly, our results highlighted the key engagement of the ipsilateral sensorimotor cortex in motor learning encoding, which deserves further investigation in future studies.

Materials and Methods

The present study is a secondary analysis of a publicly available dataset (OpenNeuro, accession number ds002776) that has been published elsewhere (9). The experimental description below was obtained from publicly available resources, such as the original publication (9) and the dataset description. Specific parts irrelevant to the present study (e.g., behavioral test sessions outside the MRI, free-speed execution) have been omitted for clarity purposes. For a full description of the experimental design, refer to the original publication (9).

Participants

In the present study, we used fMRI and behavioral data of 13 healthy participants (9 females, mean age of 21.4 (sd=2.36)) who were part of group 1 in the original dataset, and after exclusion of one participant (sub-24) due to the high amount of errors during the task-based fMRI. All participants were right-handed, had no prior history of psychiatric or neurologic disorders, and provided written informed consent to all procedures and data usage. The experimental procedures were approved by the Ethics Committee at Western University, where the data has been collected.

Training protocol

The training protocol consisted of training the execution of six 9-digit finger sequences, for five weeks, as fast as possible. Participants received feedback based on the accuracy and movement time, both online and after each trial, respectively. Each sequence was executed twice in a row, first with visual cues indicating the finger-tapping sequence, then without visual aid. Each training block consisted of 24 trials (4 trials per trained sequence) and was alternated with rest periods. The training protocol occurred 3 days per week in the first 4 weeks, and on one day in the last week. The trained sequences have been practiced for around 4000 trials in total.

Imaging acquisition

MRI data have been acquired using a 7-Tesla Siemens Magnetom scanner with a 32-receive channel head coil (8-channel parallel transmit). Anatomical T1-weighted scan used a magnetization-prepared rapid gradient echo sequence (MPRAGE) with a voxel size of 0.75 x 0.75 x 0.75 mm isotropic (field of view = 208 x 157 x 110 mm [A-P; R-L; F-H], encoding direction coronal). For fMRI data, the GRAPPA3 sequence (multiband acceleration factor 2, repetition

time [TR]=1.0 s, echo time [TE]=20 ms, flip angle [FA]=30 deg, 44 slices with isotropic voxel size of 2 x 2 x 2 mm) has been used. Gradient echo field map has been collected to estimate magnetic field inhomogeneities (transversal orientation, field of view 210 210 160 mm and 64 slices with 2.5 mm thickness, TR = 475 ms, TE = 4.08 ms, FA = 35 deg).

Experimental design

In the present study, we analyzed data from two different scanning sessions: one before and one after the five weeks of training. Each scanning session consisted of eight functional runs with an event-related design, randomly intermixing execution of trained and untrained sequences. Each sequence was repeated twice in a row, for three times within a run. Trials started with 1 s preparation time, during which the sequence was presented on the screen. After that time, a ‘go’ signal was displayed as a short pink and expanding line underneath the sequence numbers that indicated the speed at which participants were required to press along. The execution phase, including the feedback on overall performance, lasted for 3.5 s, and the inter-trial interval was 0.5 s. Each trial lasted for 5 s. Five periods of rest, each 10 s long, were added randomly between trials in each run.

Data preprocessing

Data has been preprocessed using fmriprep version 24.0.0. T1w images were corrected for intensity non-uniformity and used as T1w-reference throughout the workflow. The T1w-reference was then skull-stripped, and brain tissue segmentation of cerebrospinal fluid (CSF), white-matter (WM), and gray matter (GM) was performed. Non-linear spatial normalization to the standard space (MNI152NLin2009cAsym) was performed using brain-extracted versions of both T1w reference and the T1w template. Head motion parameters, including six rotation and translation components and transformation matrices, were estimated relative to this reference image before any spatiotemporal filtering.

Subsequently, the BOLD reference image was co-registered to the T1-weighted (T1w) anatomical reference using boundary-based registration with six degrees of freedom. Framewise displacement (FD) and DVARS metrics were calculated for each functional run. Additionally, mean signals were extracted from cerebrospinal fluid (CSF), white matter (WM), and whole-brain masks. Temporal high-pass filtering (using a discrete cosine filter with a 128-second cutoff) was applied to the preprocessed BOLD time series before principal component analyses for both anatomical (aCompCor) and temporal (tCompCor) CompCor decompositions. For aCompCor, probabilistic tissue masks for CSF, WM, and a combined CSF+WM mask were generated in anatomical space. Additional nuisance regressors included temporal derivatives and quadratic expansions of motion parameters and global signals.

Data analysis

After preprocessing, BOLD images were analyzed using Python libraries, such as nilearn, neuroboros, nibabel, and nltools. The surface-based first-level general linear model (GLM) was implemented using Nilearn's FirstLevelModel and incorporated task-related regressors for each condition, confound regressors, and an SPM hemodynamic response function (HRF) model. An autoregressive (AR1) noise model was specified. The confound regressors included WM signal, global signal, FD, and six motion parameters (translational and

rotational), which were calculated with fmriprep. Task timing and event details were extracted from event files, which specified the onset, duration, and condition of each trial. Each trial (modeled with a 3.5s length) was assigned a unique condition label combining sequence type (trained or untrained), sequence number (1-12), and pair of repetitions (from 1 to 3). In each run, contrasts were computed to estimate task-related activation. The resulting z-maps for each condition (e.g., trained_6_pair1) were then masked for the sensorimotor cortex (17) and used for the decoding analysis. In order to consider only perfectly executed trials but keeping the homogenous and balanced data structure, we selected the first 12 conditions (6 trained, 6 untrained) of each participant and run. The remaining data was discarded and not used in our analyses.

Searchlight hyperalignment

Inside each disk of radius 20 mm, hyperalignment was performed to align the neural representations across participants to a common representational space. For each fold in the leave-one-subject-and-run-out cross-validation scheme, all runs but one from the training data were used to construct the representation space. This was achieved using a Procrustes-based algorithm, which iteratively transforms the training data into a shared representational space (common space) while preserving the geometry of individual neural patterns (25). After creating the hyperalignment model inside each cortical disk using the training data, the test data (the left-out run of the left-out subject) was projected into the common space. This ensured that the test data were represented within the same common space as the training data, enabling direct comparisons. We repeated this scheme independently for each decoding model (training effect, transfer effect, resultant motor engrams) in such a way that each run of each subject was used as test data once, resulting in 104 folds.

Searchlight decoder implementation

A searchlight-based linear support vector machine (SVM) with L1 regularization was used as the decoding algorithm to classify neural activity patterns in cortical disks of radius 10 mm. The decoder was trained on the hyperaligned training data and their corresponding labels, and then tested on the hyperaligned test data. We used principal component analysis for dimensionality reduction inside each searchlight. Classification accuracies from each searchlight were placed into their center surface nodes, resulting in one accuracy map for each cross-validation fold. We used permutation testing for statistical thresholding by first repeating the analysis 100 times with randomly shuffled sequence identity labels in each searchlight. For each hemisphere and vertex, we aggregated individual-level decoding accuracies from cross-validation folds. The empirical null distribution was obtained by sampling decoding accuracies from permutation-based analyses (i.e., models tested on data with randomized labels). For each vertex, we drew bootstrap samples randomly with replacements from the pool of permutation scores. We repeated this procedure 10,000 times, each time computing the mean of the sampled values to create a distribution of group-level means under the null hypothesis. Observed decoding performance at each vertex was then compared against its corresponding null distribution. The empirical P values were computed by counting the proportion of null distribution values greater than or equal to the observed decoding accuracy, adding one to both the numerator and denominator to avoid zero probabilities and reduce bias. This constitutes a

one-sided non-parametric test for above-chance performance. The Benjamini–Hochberg procedure was subsequently applied to correct P values for multiple comparisons.

A similar approach was applied to compute the difference in classification accuracy between the training and transfer effects: we averaged the accuracy values from the 104 cross-validation folds for the two models independently, and then set accuracy values below the chance level to 50% to avoid noise and artificial inflation of the difference (16). The same procedure was applied 10,000 times to the permuted cross-validation folds, generating a null distribution of difference values for each searchlight. A two-sided P value was computed by counting how many times the absolute value of the null distribution exceeded the absolute value of the original unpermuted difference map (adding 1 to both the numerator and denominator). The Benjamini–Hochberg procedure was subsequently applied to correct P values for multiple comparisons

Statistical Analysis

For each participant, we calculated the mean accuracy per cortical area and estimated the group-level 95% confidence interval based on bootstrapping (random sampling, k = 1,000 with replacement). Repeated-measures ANOVAs were performed on the mean accuracy and laterality index (dependent variables) with condition (trained, untrained) and cortical label (anterior and superior parts of the precentral sulcus, precentral gyrus, central sulcus, postcentral sulcus, and postcentral gyrus) as within-subjects factors, and subjects as the random factor.

Using hyperalignment, the decoding models led to significant findings in most vertices after permutation testing and FDR (Benjamini–Hochberg) correction. The accuracy values closest to zero that passed the statistical threshold were: 75.4% and 69.9% for the training effect; 73% and 75.1% for the transfer effect; 0.12% (positive) /-0.12% (negative) and 0.04% (positive) / -0.08% (negative) for the difference between them, and 60.3% and 59.1% for the comparison of the resultant motor engrams, in the right and left hemispheres, respectively. As mentioned, the ROI analysis and LI were conducted on the statistically significant vertices only, and the accuracy maps were thresholded arbitrarily to improve plots visualization.

Data Availability

The fMRI data is publicly available (OpenNeuro, accession number ds002776). The codes used in this publication will be made publicly available after peer review and publication.

References

1. J. W. Krakauer, A. M. Hadjiosif, J. Xu, A. L. Wong, A. M. Haith, Motor learning. *Compr. Physiol.* **9**, 613–663 (2019).

2. S. Pau, G. Jahn, K. Sakreida, M. Domin, M. Lotze, Encoding and recall of finger sequences in experienced pianists compared with musically naïve controls: A combined behavioral and functional imaging study. *NeuroImage* **64**, 379–387 (2013).

3. R. E. Shimizu, A. D. Wu, B. J. Knowlton, Cerebellar activation during motor sequence learning is associated with subsequent transfer to new sequences. *Behav. Neurosci.* **130**, 572–584 (2016).

4. R. D. Seidler, D. C. Noll, Neuroanatomical Correlates of Motor Acquisition and Motor Transfer. *J. Neurophysiol.* **99**, 1836–1845 (2008).

5. J. Langan, R. D. Seidler, Age differences in spatial working memory contributions to visuomotor adaptation and transfer. *Behav. Brain Res.* **225**, 160–168 (2011).

6. G. Torres-Oviedo, A. J. Bastian, Seeing Is Believing: Effects of Visual Contextual Cues on Learning and Transfer of Locomotor Adaptation. *J. Neurosci.* **30**, 17015–17022 (2010).

7. G. Torres-Oviedo, A. J. Bastian, Natural error patterns enable transfer of motor learning to novel contexts. *J. Neurophysiol.* **107**, 346–356 (2012).

8. J. Diedrichsen, K. Kornysheva, Motor skill learning between selection and execution. *Trends Cogn. Sci.* **19**, 227–233 (2015).

9. E. Berlot, N. J. Popp, J. Diedrichsen, A critical re-evaluation of fMRI signatures of motor sequence learning. *eLife* **9**, 1–24 (2020).

10. A. Yokoi, S. A. Arbuckle, J. Diedrichsen, The Role of Human Primary Motor Cortex in the Production of Skilled Finger Sequences. *J. Neurosci.* **38**, 1430–1442 (2018).

11. J. V. Haxby, J. S. Guntupalli, S. A. Nastase, M. Feilong, Hyperalignment: Modeling shared information encoded in idiosyncratic cortical topographies. *eLife* **9**, 1–26 (2020).

12. P. Borovska, B. de Haas, Individual gaze shapes diverging neural representations. *Proc. Natl. Acad. Sci.* **121**, e2405602121 (2024).

13. M. Feilong, S. A. Nastase, J. S. Guntupalli, J. V. Haxby, Reliable individual differences in fine-grained cortical functional architecture. *NeuroImage* **183**, 375–386 (2018).

14. H. Jung, *et al.*, Action features dominate cortical representation during natural vision. [Preprint] (2025). Available at: https://www.biorxiv.org/content/10.1101/2025.01.30.635800v1 [Accessed 4 June 2025].

15. V. Taschereau-Dumouchel, *et al.*, Towards an unconscious neural reinforcement intervention for common fears. *Proc. Natl. Acad. Sci. U. S. A.* **115**, 3470–3475 (2018).

16. M. Visconti di Oleggio Castello, J. V. Haxby, M. I. Gobbini, Shared neural codes for visual and semantic information about familiar faces in a common representational space. *Proc. Natl. Acad. Sci.* **118**, e2110474118 (2021).

17. C. Destrieux, B. Fischl, A. Dale, E. Halgren, Automatic parcellation of human cortical gyri and sulci using standard anatomical nomenclature. *NeuroImage* **53**, 1–15 (2010).

18. R. D. Seidler, Neural Correlates of Motor Learning, Transfer of Learning, and Learning to Learn. *Exerc. Sport Sci. Rev.* **38**, 3 (2010).

19. E. Berlot, N. J. Popp, S. T. Grafton, J. Diedrichsen, Combining Repetition Suppression and Pattern Analysis Provides New Insights into the Role of M1 and Parietal Areas in Skilled Sequential Actions. *J. Neurosci.* **41**, 7649–7661 (2021).

20. E. Dayan, L. G. Cohen, Neuroplasticity subserving motor skill learning. *Neuron* **72**, 443–454 (2011).

21. C. Kelly, J. J. Foxe, H. Garavan, Patterns of Normal Human Brain Plasticity After Practice and Their Implications for Neurorehabilitation. *Arch. Phys. Med. Rehabil.* **87**, 20–29 (2006).

22. R. M. Hardwick, C. Rottschy, R. C. Miall, S. B. Eickhoff, A quantitative meta-analysis and review of motor learning in the human brain. *NeuroImage* **67**, 283–297 (2013).

23. C. J. Steele, V. B. Penhune, Specific Increases within Global Decreases: A Functional Magnetic Resonance Imaging Investigation of Five Days of Motor Sequence Learning. *J. Neurosci.* **30**, 8332–8341 (2010).

24. J. V. Haxby, A. C. Connolly, J. S. Guntupalli, Decoding Neural Representational Spaces Using Multivariate Pattern Analysis. *Annu. Rev. Neurosci.* **37**, 435–456 (2014).

25. J. V. Haxby, *et al.*, A Common, High-Dimensional Model of the Representational Space in Human Ventral Temporal Cortex. *Neuron* **72**, 404–416 (2011).

26. T. Wiestler, J. Diedrichsen, Skill learning strengthens cortical representations of motor sequences. *eLife* **2013** (2013).

27. K. Kornysheva, J. Diedrichsen, Human premotor areas parse sequences into their spatial and temporal features. *eLife* **3**, e03043 (2014).

28. B. Garzón, *et al.*, Cortical changes during the learning of sequences of simultaneous finger presses. *Imaging Neurosci.* **1**, 1–26 (2023).

29. M.-H. Monfils, E. J. Plautz, J. A. Kleim, In Search of the Motor Engram: Motor Map Plasticity as a Mechanism for Encoding Motor Experience. *The Neuroscientist* **11**, 471–483 (2005).

30. I. Nambu, *et al.*, Decoding sequential finger movements from preparatory activity in higher-order motor regions: a functional magnetic resonance imaging multi-voxel pattern analysis. *Eur. J. Neurosci.* **42**, 2851–2859 (2015).

31. J. Xiong, *et al.*, Long-term motor training induced changes in regional cerebral blood flow in both task and resting states. *NeuroImage* **45**, 75–82 (2009).

32. L. Ma, *et al.*, Changes in regional activity are accompanied with changes in inter-regional connectivity during 4 weeks motor learning. *Brain Res.* **1318**, 64–76 (2010).

33. V. B. Penhune, J. Doyon, Dynamic Cortical and Subcortical Networks in Learning and Delayed Recall of Timed Motor Sequences. *J. Neurosci.* **22**, 1397–1406 (2002).

34. C. Horenstein, M. J. Lowe, K. A. Koenig, M. D. Phillips, Comparison of unilateral and bilateral complex finger tapping-related activation in premotor and primary motor cortex. *Hum. Brain Mapp.* **30**, 1397–1412 (2009).

35. D. A. Nowak, C. Grefkes, M. Ameli, G. R. Fink, Interhemispheric competition after stroke: Brain stimulation to enhance recovery of function of the affected hand. *Neurorehabil. Neural Repair* **23**, 641–656 (2009).

36. M. Kobayashi, H. Théoret, A. Pascual-Leone, Suppression of ipsilateral motor cortex facilitates motor skill learning. *Eur. J. Neurosci.* **29**, 833–836 (2009).

37. B. W. Vines, D. G. Nair, G. Schlaug, Contralateral and ipsilateral motor e¡ects after transcranial direct current stimulation. *NeuroReport* **17**, 672–674 (2006).

38. J. Duque, *et al.*, Transcallosal inhibition in chronic subcortical stroke. *NeuroImage* **28**, 940–946 (2005).

39. M. L. Harris-Love, E. Chan, A. W. Dromerick, L. G. Cohen, Neural Substrates of Motor Recovery in Severely Impaired Stroke Patients With Hand Paralysis. *Neurorehabil. Neural Repair* **30**, 328–338 (2016).

40. N. Murase, J. Duque, R. Mazzocchio, L. G. Cohen, Influence of interhemispheric interactions on motor function in chronic stroke. *Ann. Neurol.* **55**, 400–409 (2004).

41. A. Keitel, H. Øfsteng, V. Krause, B. Pollok, Anodal Transcranial Direct Current Stimulation (tDCS) Over the Right Primary Motor Cortex (M1) Impairs Implicit Motor Sequence Learning of the Ipsilateral Hand. *Front. Hum. Neurosci.* **12** (2018).

42. R. Hamel, *et al.*, Bilateral intracortical inhibition during unilateral motor preparation and sequence learning. *Brain Stimulat.* **17**, 349–361 (2024).

43. J. Diedrichsen, T. Wiestler, J. W. Krakauer, Two Distinct Ipsilateral Cortical Representations for Individuated Finger Movements. *Cereb. Cortex* **23**, 1362–1377 (2013).

44. E. Berlot, G. Prichard, J. O'Reilly, N. Ejaz, J. Diedrichsen, Ipsilateral finger representations in the sensorimotor cortex are driven by active movement processes, not passive sensory input. *J. Neurophysiol.* **121**, 418–426 (2019).

45. T. Wiestler, S. Waters-Metenier, J. Diedrichsen, Effector-independent motor sequence representations exist in extrinsic and intrinsic reference frames. *J. Neurosci. Off. J. Soc. Neurosci.* **34**, 5054–5064 (2014).

46. S. Waters, T. Wiestler, J. Diedrichsen, Cooperation Not Competition: Bihemispheric tDCS and fMRI Show Role for Ipsilateral Hemisphere in Motor Learning. *J. Neurosci.* **37**, 7500–7512 (2017).

47. Y. Huang, *et al.*, Motor Training Increases the Stability of Activation Patterns in the Primary Motor Cortex. *PLoS ONE* **8**, e53555 (2013).

48. J. Kolasinski, *et al.*, The dynamics of cortical GABA in human motor learning. *J. Physiol.* **597**, 271–282 (2019).

49. W. Muellbacher, *et al.*, Early consolidation in human primary motor cortex. *Nature* **415**, 640–644 (2002).

50. N. Picard, Y. Matsuzaka, P. L. Strick, Extended practice of a motor skill is associated with reduced metabolic activity in M1. *Nat. Neurosci.* **16**, 1340–1347 (2013).

51. Y. Matsuzaka, N. Picard, P. L. Strick, Skill Representation in the Primary Motor Cortex After Long-Term Practice. *J. Neurophysiol.* **97**, 1819–1832 (2007).

52. A.-K. Gellner, J. Reis, B. L. Fiebich, B. Fritsch, Cx3cr1 deficiency interferes with learning- and direct current stimulation-mediated neuroplasticity of the motor cortex. *Eur. J. Neurosci.* **59**, 177–191 (2024).

53. A. Karni, *et al.*, Functional MRI evidence for adult motor cortex plasticity during motor skill learning. *Nature* **377**, 155–158 (1995).

Supplementary Information

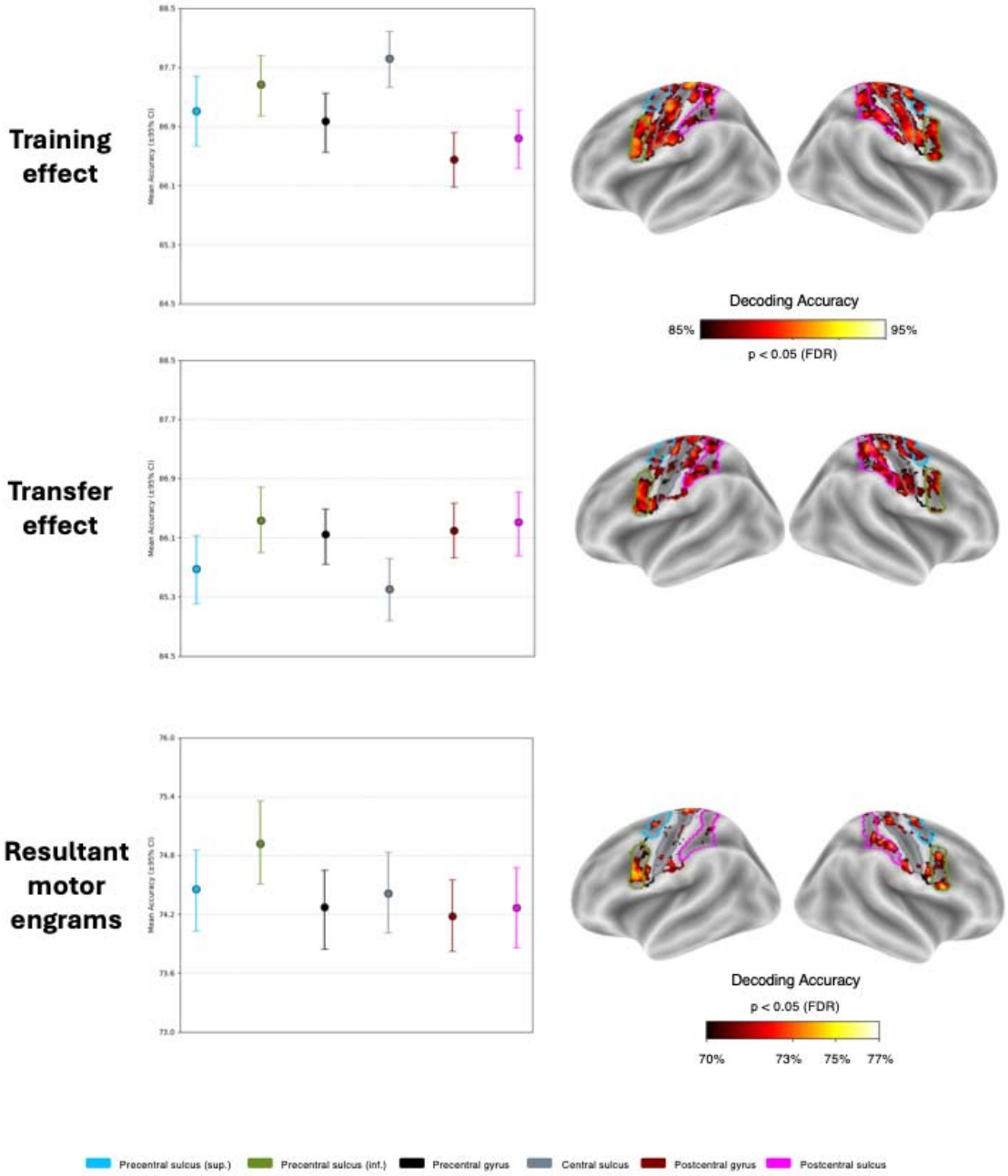

Figure S1. Mean accuracy and confidence interval (95%) obtained with bootstrapping in both decoding models.

Between-subject decoding models with anatomically aligned data

When compared to the decoding models that used hyperaligned data, between-subject decoding models with anatomically aligned data revealed limited decoder accuracy (Figure S2). These analyses followed the same procedure as their counterparts on hyperaligned data,

except that the individual functional data were kept in the template surface fsaverage. For the anatomically aligned models, the training effect identified 1,023 (left) and 1,168 (right) supra-threshold vertices, whereas the transfer effect yielded 0 (left) and 23 (right), and the motor engrams model produced 498 (left) and 23 (right). Across all models, hyperalignment improved decoder accuracy in 100% of the vertices.

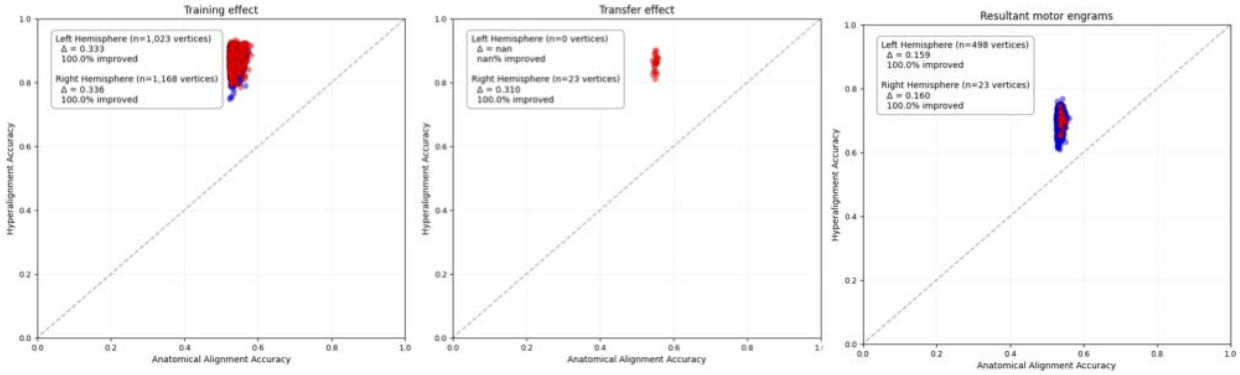

Figure S2. Scatterplot of searchlights' accuracies for each decoding model. Between-subject classification with anatomically aligned data did not result in a robust decoding model.